Dielectric spectroscopy of confinement effects in polar materials

R. Pelster
II. Physikalisches Institut der Universität zu Köln, Zülpicher Straße 77, D-50937 Köln, Germany
(Received 4 September 1998)

Spatial confinement on a nm scale can affect molecular dynamics changing form, strength, and frequency of relaxation processes. Dielectric spectroscopy can reveal confinement effects, however, an effective medium analysis has to remove the effects of dielectric heterogeneity. Depending on the microstructure they cause remarkable discrepancies between the intrinsic and measured effective properties. Here, the theoretical response of various three-dimensional (3D), 2D, and 1D confinements is analyzed: molecules in dispersed droplets, noncrossing or interconnected channels, and films. Experimental data on the α relaxation of confined propylene glycol reflect both the microstructure and the molecular reorientation, but effects of dielectric heterogeneity can be separated from finite-size and surface effects. While randomly distributed nanodroplets correspond to a well-defined 3D confinement, porous Gelsil glass exhibits a transition from a 2D to a 2D-3D topology with decreasing porosity and pore size. Nonuniform interaction with the surface or surface attached molecules essentially affects only the shape of the α process and results in a broadening. The relaxation of the confined liquid becomes faster and its glass transition temperature is lowered. The diameter above which the finite-size effect vanishes does not depend on geometrical details or chemical nature of the confinement and characterizes the dynamics of the liquid. [S0163-1829(99)04013-8]

The molecular behavior of spatially confined materials can be probed on length scales down to a few nm. Especially glass-forming liquids, polymers, and liquid crystals have been the center of attention for the last few years.[1–17] Dynamic experiments focus on the question of whether the molecular relaxations in a restricted geometry differ from those of the bulk state. Various mechanisms can induce changes of the molecular dynamics, and all of them may vary with the size of the confinement.

(i) Structural effects due to steric hindrance in the finite volume: an example is an induced chain orientation of polymers in thin films,[2] but also a reduced density as a result of difficulty in packing the molecules might be at least conceivable.[4]

(ii) Surface effects: a modified molecular interaction at the boundaries of the confinement may be restricted to a surface layer[6,18] or even extend into the confined volume. For example, water at hydrophilic surfaces exhibits an increased hydrogen bond connectivity that is effective up to a capillary size of 10 nm.[19] It enhances the viscosity and slows down the orientational relaxation.

(iii) Finite-size effects due to spatial heterogeneity of the confined material: these occur, for example, when the geometrically imposed length scale d becomes smaller than an intrinsic length scale characterizing the dynamics of the bulk material. In glass formers, intrinsic nanoscale heterogeneity is an important concept.[7] Cooperative nanoregions are thought to constitute a length scale ξ relevant for the vitrification process.[20] Recent experiments hint at a high coupling between neighboring regions.[15] In any case, the nonexponential dynamics of the α relaxation does not arise from a simple superposition of independent exponential processes.[16] Even though the underlying mechanism is disputed, a geometrical confinement on a nm scale has been shown to speed up the α relaxation and to lower the glass transition temperature.[3,4,6,8–11]

In order to distinguish between the above effects, that may superpose or even supress each other,[6] the type of confinement may be varied in an experiment, i.e., chemical nature, size, and number of confined dimensions.[6,8–11] Various techniques such as differential scanning calorimetry, dielectric spectroscopy, solvation dynamics, NMR, neutron scattering, and light scattering have been used (see citations in Ref. 7). Dielectric spectroscopy is appropriate for the investigation of polar materials and covers a large dynamical range from dc up to microwaves. It provides information on the molecular reorientation, *inter alia* on relaxation frequencies, activation energies, and molecular interactions. The difficulty with the interpretation of experiments on a filler confined in a matrix is that dielectric spectroscopy does not act as a local probe but measures the effective dynamics of the whole system. Neither the permittivity of the filler ε_p nor that of the matrix ε_m is obtained but a volume-averaged effective value is. It is well defined as long as the wavelength of the electric field $\mathbf{E}$ is much larger than the length scale of the inhomogenieties: $\varepsilon_{\rm eff}\langle\mathbf{E}(\mathbf{r})\rangle=\langle\varepsilon(\mathbf{r})\mathbf{E}(\mathbf{r})\rangle$, where $\langle\cdots\rangle$ denotes the volume average. This definition can be rewritten in terms of the averaged fields in the respective components[21,22]

$$\varepsilon_{\rm eff}=\frac{(1-f)\varepsilon_m+f\varepsilon_p\langle E\rangle_p/\langle E\rangle_m}{(1-f)+f\langle E\rangle_p/\langle E\rangle_m}, \tag{1}$$

where $f=V_p/V_{\rm total}$ is the volume filling factor. In contrast to measurements on the pure filler (bulk), the electric field distribution is inhomogeneous. The ratio $\langle E\rangle_p/\langle E\rangle_m$ and thus the measured effective permittivity depends on the microstructure, i.e., on topology, degree of order, and dimensionality. The permittivity of the filler and with it intrinsic relaxation frequencies and strengths as well as the form of the relaxation function are only obtained via an effective medium analysis. This work is a systematic study of various

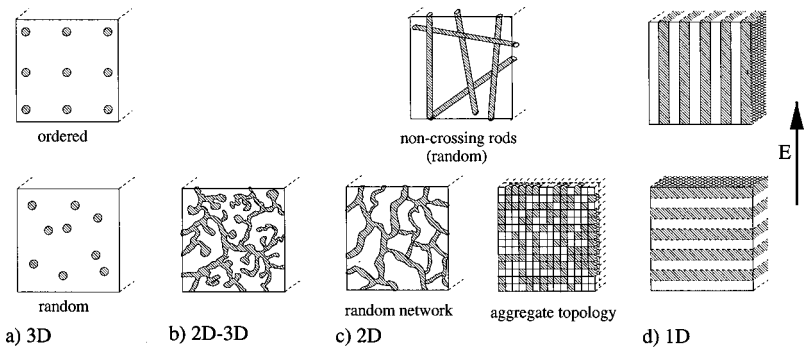

FIG. 1. Sketch of various confinements. The number of confined dimensions varies but the effective system always extends in three dimensions. (a) 3D confined droplets. (b) 2D-3D confined pores with a high amount of dead ends and/or a fractally rough surface. (c) 2D confined continuous pores running right through the whole sample: noncrossing straight rods and network of interconnected curved pores. The latter one is approximated by a random distribution of matrix and filler material on a cubic grid (aggregate topology for $f>f_c=0.33$). (d) 1D confined layers or films.

structures, in which a polar material is confined in one, two, or three dimensions (see Fig. 1): droplets [three-dimensional (3D) confinement], noncrossing pores and networks (2D), and films or multilayers (1D). In this notation D refers to the confining dimensionality while the complementary filler dimensionality 3-D corresponds to the number of unrestricted dimensions. In addition to a theoretical analysis of $\varepsilon_{\rm eff}$, experimental data on a glass-forming liquid confined to nanopores and nanodroplets is discussed (see Fig. 2). The aim is to show how effects of dielectric heterogeneity, i.e., simple mixture effects, can be reliably separated from finite-size or surface effects. To a certain degree this is even possible when the detailed information on the microstructure is not available or has to be derived from the dielectric data.

I. 3D CONFINEMENT

In general, the complex permittivity of a material, $\varepsilon_p=\varepsilon_p'-i\varepsilon_p''$, depends on both frequency ν and temperature T. At low frequencies it may be measured via the complex capacitance of a material-filled condenser $C_{\rm mat}=\varepsilon_p\cdot C_0$, where C_0 denotes the capacitance of the empty cell. We start our analysis with a filler having a relaxation of the Cole-Cole form[24,25]

$$\varepsilon_p(\nu)=\varepsilon_{p,\infty}+\frac{\Delta\varepsilon_p}{1+[i(\nu/\nu_p)]^{1-\alpha}}, \tag{2}$$

where $\varepsilon_{p,\infty}$ denotes the high frequency permittivity. The three parameters characterizing the relaxation process, i.e., relaxation frequency ν_p, relaxation strenght $\Delta\varepsilon_p$, and shape α, generally depend on temperature. $\Delta\varepsilon_p$ is a measure for the dipole moment and the number of molecules taking part in the relaxation. The imaginary part of ε_p is due to the dissipation of energy. It shows a symmetric relaxation peak with a maximum at the relaxation frequency ν_p, which yields the relaxation time $\tau_p=1/(2\pi\nu_p)$. ν_p characterizes the reorientational dynamics in an alternating field. Its temperature dependence allows us to determine, e.g., the height of potential barriers hindering changes of the dipole direction.[26] The parameter α describes the form of the relaxation. For $\alpha=0$ this is a Debye-like relaxation with a half width of 1.14 frequency decades [in the time domain this corresponds to an

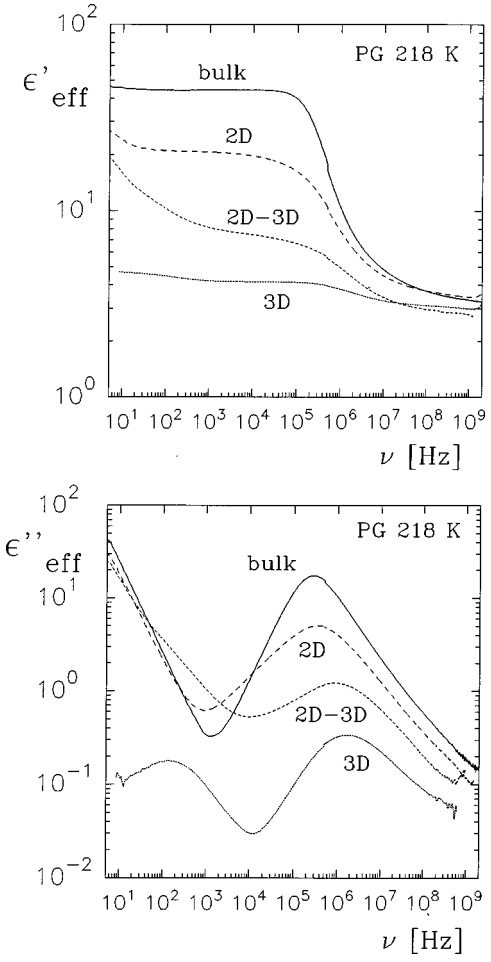

FIG. 2. Complex permittivity $\varepsilon_{\rm eff}=\varepsilon_{\rm eff}'-i\varepsilon_{\rm eff}''$ vs frequency for propylene glycol in the bulk state ($\varepsilon_{\rm eff}=\varepsilon_p$) and in confinements. The measurements were performed at 218 K: (2D) Gelsil glass with porosity 70% and pore diameter 7.5 nm, (2D-3D) Gelsil glass with porosity 63% and pore diameter 5 nm, and (3D) butyl rubber with nanodroplets (10.2 nm, 16.4 vol. %). For details see Secs. I D and II C. Besides the number of confined dimensions also filling factor and surface interaction differ. Above 10 kHz the α relaxation is visible. Below 1 kHz the imaginary part of the bulk values is governed by dc conductivity $\varepsilon_p''=\sigma_p/(\varepsilon_0\omega)$, causing interfacial polarization phenomena in the confined systems that depend on the microstructure as well (Ref. 23).

exponential decay of a polarization $P(t) \propto \exp(t/\tau_p)$]. For $0 < \alpha < 1$ a deviation from the Debye form due to a symmetric broadening of the relaxation peak is observed, while the peak height $\varepsilon''_{\max}$ decreases (the unsymmetrical case is treated in Sec. I C). This broadening either arises from a hierarchical non-Debye process of interacting molecules[27] or from a superposition of independent Debye-like relaxations.[25,26] In the latter case ν_p can be interpreted as the mean relaxation frequency.

When particles of the above material are dispersed in a continuous medium [see Fig. 1(a)], a so-called matrix inclusion topology is obtained (cermet topology, separated grain structure). It describes suspensions, emulsions, and filled polymers,[28] where matrix and filler are not topologically equivalent.[21] In contrast to the filler we assume the matrix to have no losses, i.e., its permittivity ε_m is independent of frequency and a real number. Even if a homogeneous electric field is applied, the local field acting on each particle is inhomogeneous. It is the superposition of the external field and of the induced fields of the surrounding polarized particles. In general, dipole as well as multipole fields are induced. The higher the filling factor, the more important the spatial distribution of the particles. We first consider the limit of low filling factors, where such structural aspects are negligible.

A. Dilute inclusions

In dilute systems of nonagglomerating particles the distances between the particles are large and they are exposed to an approximately uniform electric field. In spheres or in orientated ellipsoids only dipole moments are induced. For such systems the effective permittivity is independent of the exact spatial distribution of the particles

$$\varepsilon_{\text{eff}} = \varepsilon_m \left(1 + \frac{1}{A} \frac{fx}{1-fx} \right) \quad \text{for} \quad f|x| \ll 1 \tag{3}$$

holds, where

$$x = \frac{A(\varepsilon_p - \varepsilon_m)}{A(\varepsilon_p - \varepsilon_m) + \varepsilon_m}. \tag{4}$$

For spherical particles $A = 1/3$ and Eq. (3) is the Maxwell-Garnett formula. Sillars extended it to the general case of orientated ellipsoids,[29,30] where the depolarization factor A depends on the shape of the particle $(0 \leqslant A \leqslant 1)$. It is a measure for the ratio of the mean field inside and outside a polarized particle:

$$\frac{\langle E \rangle_p}{\langle E \rangle_m} = \frac{\varepsilon_m}{A(\varepsilon_p - \varepsilon_m) + \varepsilon_m} \tag{5}$$

[compare Eqs. (1) and (3)]. We keep this general notation, since it will be used later. However, in this section we only consider spheres [Fig. 1(a)]. In the case of conducting particles Eq. (3) yields the well-known Maxwell-Wagner-Sillars formula describing an interfacial polarization process due to charge accumulation.[23,29,30] However, we assume a particle permittivity according to Eq. (2), where the contribution of the dc conductivity $-i\sigma_p/(\varepsilon_0 2\pi\nu)$ is negligibly small in the frequency range of the orientational dynamics. This also implies that a possible interfacial polarization process appears at frequencies far below ν_p and does not impede the experimental observation of the molecular relaxation (see Fig. 2). Inserting Eq. (2) in Eq. (3) yields an effective permittivity

$$\varepsilon_{\text{eff}} = \varepsilon_{\text{eff},\infty} + \frac{\Delta\varepsilon_{\text{eff}}}{1 + [i(\nu/F\nu_p)]^{1-\alpha}}, \tag{6}$$

i.e., the form of the relaxation process remains unchanged. $F = \nu_{\text{eff}}/\nu_p = \tau_p/\tau_{\text{eff}}$ denotes the shift of the relaxation frequency[31]

$$F = \left(1 + \Delta\varepsilon_p \frac{A(1-f)}{\varepsilon_m + A(1-f)(\varepsilon_{p,\infty} - \varepsilon_m)} \right)^{1/(1-\alpha)} \geqslant 1, \tag{7}$$

and

$$\Delta\varepsilon_{\text{eff}} = \frac{f\Delta\varepsilon_p \varepsilon_m^2}{\{\varepsilon_m + A(1-f)(\Delta\varepsilon_p + \varepsilon_{p,\infty} - \varepsilon_m)\}\{\varepsilon_m + A(1-f)(\varepsilon_{p,\infty} - \varepsilon_m)\}}, \tag{8}$$

$$\varepsilon_{\text{eff},\infty} = \varepsilon_m \left(1 + f \frac{\varepsilon_{p,\infty} - \varepsilon_m}{\varepsilon_m + A(1-f)(\varepsilon_{p,\infty} - \varepsilon_m)} \right). \tag{9}$$

The frequency shift is a consequence of dielectric heterogeneity. According to Eq. (5) the mean fields in matrix and filler differ. Since ε_p is a complex quantity, there is also a phase shift. It affects the frequency of maximum loss [see Eq. (1)], i.e., the effective relaxation frequency and thus $\nu_{\text{eff}} \geqslant \nu_p$ [Eq. (7)]. This is a pure effective medium effect that does not imply any finite-size or surface induced changes of the molecular behavior, i.e., of $\Delta\varepsilon_p$ or ν_p. The shift F becomes more pronounced with increasing relaxation strength $\Delta\varepsilon_p$ or broadening α of the intrinsic relaxation. It reaches its maximum value for $f \to 0$ and can be of the order of one frequency decade [see Fig. 3(c)]. In addition to the frequency shift F also the effective relaxation strength increases with increasing $\Delta\varepsilon_p$. In the case of strongly polar materials, where $\Delta\varepsilon_p \gg \varepsilon_m/[A(1-f)]$, $|\varepsilon_{p,\infty} - \varepsilon_m|$, Eqs. (7) and (8) yield

$$F \propto \Delta\varepsilon_p^{1/(1-\alpha)}, \tag{10}$$

$$\Delta\varepsilon_{\text{eff}} = \frac{f}{A(1-f)} \frac{\varepsilon_m}{1 + A(1-f)(\varepsilon_{p,\infty}/\varepsilon_m - 1)} \ll \Delta\varepsilon_p. \tag{11}$$

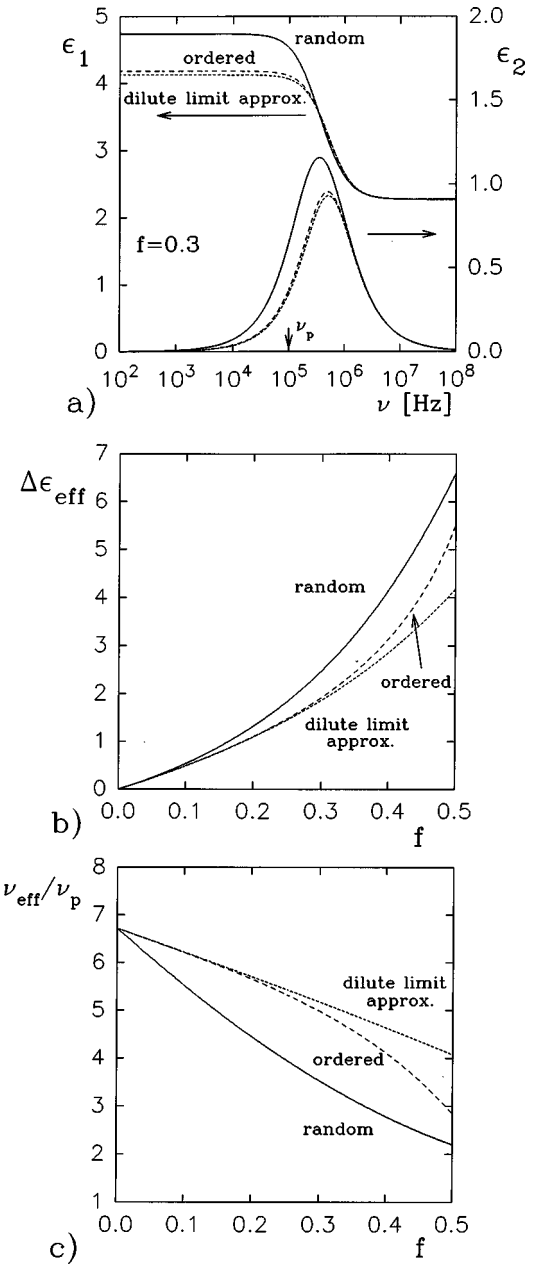

FIG. 3. Relaxation process for a matrix inclusion topology of droplets with a symmetric relaxation [Eq. (2)] embedded in an insulating matrix ($A=1/3$, $\Delta\varepsilon_p=40$, $\varepsilon_{p,\infty}=3$, $\nu_p=10^5$ Hz, $\alpha=0$, $\varepsilon_m=2$). (a) Effective dielectric function $\varepsilon_{\rm eff}=\varepsilon_1-i\varepsilon_2$ vs frequency at a filling factor of $f=30\%$. (b) Effective relaxation strength $\Delta\varepsilon_{\rm eff}$ vs filling factor f. (c) Frequency shift $\nu_{\rm eff}/\nu_p$ of the effective relaxation vs filling factor. Dilute limit approximation: Eq. (3); ordered: Eq. (12) for the simple cubic lattice; random: Hanai-Bruggeman Eq. (13).

The effective relaxation strength becomes independent of $\Delta\varepsilon_p$. Only the measured relaxation frequency $\nu_{\rm eff}$, its temperature dependence, or the form of the effective relaxation contain information on the intrinsic relaxation of the filler and can be used to detect possible size effects.

B. Effects of interaction

When the filling factor increases, the local field acting on each particle becomes nonuniform and depends on the exact spatial distribution of the surrounding particles. In general, higher multipoles have to be taken into account.

First we focus on ordered systems which can be treated exactly. For a cubic lattice (sc) of spherical particles Eq. (3) has been extended to include effects of multipoles up to $n=7$ (Ref. 32):

$$\varepsilon_{\rm eff}=\varepsilon_m\left(1+3\frac{fx}{1-fx(1+M)}\right)\quad\text{for}\quad f\leqslant 0.46, \tag{12}$$

with

$$M=b_1x_5f^{11/3}+c_1x_7f^5-af^{7/3}\frac{1+c_2x_5f^{11/3}+c_3x_5^2f^{22/3}}{-x_3^{-1}+b_2f^{7/3}+c_4x_5f^6}$$

and $x_n=(\varepsilon_p-\varepsilon_m)/[\varepsilon_p+\varepsilon_m(n+1)/n]$. The coefficients are $a=1.3045$, $b_1=0.01476$, $b_2=0.4054$, $c_1=0.1259$, $c_2=0.5289$, $c_3=0.06993$, and $c_4=6.1673$. Precise numerical calculations including all higher multipoles have been carried out, e.g., in Refs. 32,33. In Fig. 3 the effective permittivity of the ordered system is compared to the dilute limit approximation, Eq. (3). The higher multipole moments result in (i) an enhanced relaxation strength and (ii) a less pronounced shift of the relaxation frequency. The deviations from the dilute limit approximation become visible above $f\simeq 0.2$.

In contrast to ordered systems, where the interparticle spacing is fixed, in random or disordered systems particles can become closer and even agglomerate. Therefore, Eq. (3) is already expected to fail at much lower filling factors. There is a variety of approximative mean-field mixture formulas for random systems of the matrix inclusion type (for a review see Refs. 21,29,30). In order to avoid an explicit calculation of the higher multipole moments, each particle is assumed to be polarized in a modified homogeneous mean field. In the Hanai-Bruggeman formula the higher concentration of spheres has been taken into account using an integral method:[29,30]

$$\frac{\varepsilon_{\rm eff}-\varepsilon_p}{\varepsilon_m-\varepsilon_p}\left(\frac{\varepsilon_m}{\varepsilon_{\rm eff}}\right)^{1/3}=1-f\quad\text{for}\quad f<f_c. \tag{13}$$

It applies below the critical filling factor f_c, at which the first continuous paths of agglomerating particles form. In any case the mean field approximation is expected to fail above $f\geqslant 0.5$, when the particles are too close together. In order to make understand the frequency dependence of $\varepsilon_{\rm eff}$ shown in Fig. 3(a), we expand Eq. (13) for the case $|\varepsilon_p|\geqslant\varepsilon_{p,\infty}\gg\varepsilon_m$, that also implies $|\varepsilon_p|\gg|\varepsilon_{\rm eff}|$ as long as f is not too large:

$$(1-f)^3\frac{\varepsilon_{\rm eff}}{\varepsilon_m}=\left(\frac{1-\varepsilon_{\rm eff}/\varepsilon_p}{1-\varepsilon_m/\varepsilon_p}\right)^3\simeq 1-3\frac{\varepsilon_{\rm eff}}{\varepsilon_p}+3\frac{\varepsilon_m}{\varepsilon_p}+\cdots \tag{14}$$

and thus

$$\varepsilon_{\rm eff}\simeq\varepsilon_m\frac{1+3\varepsilon_m/\varepsilon_p}{(1-f)^3+3\varepsilon_m/\varepsilon_p}. \tag{15}$$

Inserting a particle permittivity of the Cole-Cole type [see Eq. (2)] yields an effective permittivity of the same form [Eq. (6)] with

$$F \simeq \left(1+\Delta\varepsilon_p \frac{(1-f)^3}{3\varepsilon_m+(1-f)^3\varepsilon_{p,\infty}} \right)^{1/(1-\alpha)} \tag{16}$$

and

$$\Delta\varepsilon_{\text{eff}} \simeq \frac{9\varepsilon_m^2\Delta\varepsilon_p f(1-f+f^2/3)}{\{3\varepsilon_m+(1-f)^3(\Delta\varepsilon_p+\varepsilon_{p,\infty})\}\{3\varepsilon_m+(1-f)^3\varepsilon_{p,\infty}\}}. \tag{17}$$

As before, Eq. (10) describes the shift of the relaxation frequency of strongly polar materials, where $1/3(1-f)^3\Delta\varepsilon_p \gg \varepsilon_m$ and $\Delta\varepsilon_p \gg \varepsilon_{p,\infty}$. Equation (17) simplifies to

$$\Delta\varepsilon_{\text{eff}} \simeq \frac{1-(1-f)^3}{(1-f)^3} \frac{\varepsilon_m}{1+1/3(1-f)^3\varepsilon_{p,\infty}/\varepsilon_m} \ll \Delta\varepsilon_p, \tag{18}$$

i.e., for large $\Delta\varepsilon_p$ the effective relaxation strength becomes independent of the intrinsic relaxation process and only reflects the microstructure.

The approximative Eqs. (15)–(17) help to elucidate the general characteristics, but their numerical quality depends on whether the assumption of a large particle permittivity is fulfilled also at high frequencies, so that $\varepsilon_{p,\infty} \gg \varepsilon_m$. In the following, we always use precise results of a numerical analysis of Eq. (13) when we refer to the Hanai-Bruggeman formula. Dielectric heterogeneity of the effective medium affects the form of the relaxation process, although it is hardly visible in Fig. 3(a). The half width of the relaxation peak is about 1.245 frequency decades, i.e., it is 9% larger compared to the Cole-Cole-type relaxation of ε_p [Eq. (2)]. The effective relaxation strength is shown in Fig. 3(b). Above $f=0.05$ a deviation from the dilute limit approximation, Eq. (3), becomes visible. The frequency shift according to Eq. (13) is displayed in Fig. 3(c) [Eq. (16) would yield values with an accuracy of 15–20 %]. The dilute limit approximation clearly overestimates the shift of the relaxation frequencies, even at low f. Besides the broadening of the relaxation, the effects of particle interaction are qualitatively the same as for ordered systems but more intense: the ε_{eff}-values are enhanced and the shift of the relaxation frequency $F=\nu_{\text{eff}}/\nu_p$ is less strong.

In general, the values of ε_{eff} and the relaxation frequency ν_{relax} depend on the exact spatial distribution of the particles. When higher multipole moments become important, that is with increasing disorder or filling factor, $\Delta\varepsilon_{\text{eff}}$ increases while the frequency shift of ν_{eff} decreases [see Fig. 3(c)]. Equally, agglomeration gives rise to a broadening of the relaxation peak.[34] Exact numerical techniques are described in Refs. 34–36 (matrix inclusion topology for $f<f_c$).

C. Asymmetric relaxations

Until now we have considered confined liquids having a symmetric relaxation of the type of Eq. (2). We have shown that its shape is approximately preserved in the effective permittivity. In this section we treat the more general case of asymmetric relaxations. The permittivity of many materials can be described by the empirical Havriliak-Negami formula[37]

$$\varepsilon_p = \varepsilon_{p,\infty} + \frac{\Delta\varepsilon_p}{\{1+[i(\nu/\nu_0)]^{1-\alpha}\}^\gamma} \tag{19}$$

with shape parameters α and γ. Once again, the relaxation frequency ν_p is meant to be the frequency at which the maximum of the imaginary part is observed. $\nu_p=\nu_0$ only holds in the case of a symmetric loss peak, where $\gamma=1$ (a general expression for ν_p is given in Ref. 38). The shape parameters are related to the slope of ε_p'' on the low and the high frequency side of the normalized loss peak:

$$\frac{\varepsilon''}{\Delta\varepsilon_p}(\nu \ll \nu_p) \simeq \sin[(1-\alpha)\pi/2]\gamma\left(\frac{\nu}{\nu_0}\right)^{1-\alpha}, \tag{20}$$

$$\frac{\varepsilon''}{\Delta\varepsilon_p}(\nu \gg \nu_p) \simeq \sin[(1-\alpha)\pi/2]\left(\frac{\nu_0}{\nu}\right)^{(1-\alpha)\gamma}. \tag{21}$$

In a double-logarithmic plot $\partial\ln\varepsilon''/\partial\ln\nu = 1-\alpha$ holds for the low frequency side of the peak, while for the high frequency side $\partial\ln\varepsilon''/\partial\ln\nu = -(1-\alpha)\gamma$. The case $\alpha=0$ and $\gamma=1$ corresponds to the Debye form, while for $\gamma<1$ or $\alpha>0$ a broadening is observed. For certain values of α and γ the corresponding nonexponential decay of polarization in the time domain can be approximated by a Kohlrausch-Williams-Watts function $P(t)\propto\exp[-(t/\tau_{\text{KWW}})^\beta]$, although the latter description with one shape parameter β is less general.[43] As in the symmetric case, the broadening either arises from a hierarchical non-Debye process[27] or from a superposition of independent relaxations (parallel processes).[25,26] In the latter case

$$\varepsilon_p = \sum_i \frac{\Delta\varepsilon_{p,i}}{1+i\nu/\nu_{p,i}} + \varepsilon_{p,\infty}. \tag{22}$$

In general, different frequency shifts are expected for each component. Only for symmetric peaks the shape of the relaxation remains approximately unchanged.

In order to describe the effect of an asymmetric broadening for parallel as well as for hierarchical processes, we perform an effective medium analysis using Eq. (19). Obviously, neither the static nor the high frequency values of the permittivity are affected by the broadening. The formulas for the relaxation strength $\Delta\varepsilon_{\text{eff}} = \varepsilon_{\text{eff}}(\varepsilon_p=\Delta\varepsilon_p+\varepsilon_{p,\infty}) - \varepsilon_{\text{eff}}(\varepsilon_p=\varepsilon_{p,\infty})$, Eqs. (8) and (17), remain valid. However, the asymmetric broadening influences the shift of the relaxation frequency and the shape of the loss peak. Inserting Eq. (19) in the Maxwell-Garnett result for dilute systems [Eq. (3)] or in the Hanai-Bruggeman formula [the approximative Eq. (15)] yields an effective permittivity

$$\varepsilon_{\text{eff}} = \varepsilon_{\text{eff},\infty} + \frac{\Delta\varepsilon_{\text{eff}}}{1+\{[1+(i\nu/\nu_0)^{1-\alpha}]^\gamma - 1\}/F^{1-\alpha}}, \tag{23}$$

where F is given by Eq. (7) or (16), respectively. Only for $\gamma=1$ the effective permittivity is of the Havriliak-Negami form [Eq. (19)] and the shape of the intrinsic relaxation is preserved. In the general case, the respective low and high frequency limits of the normalized loss peak are

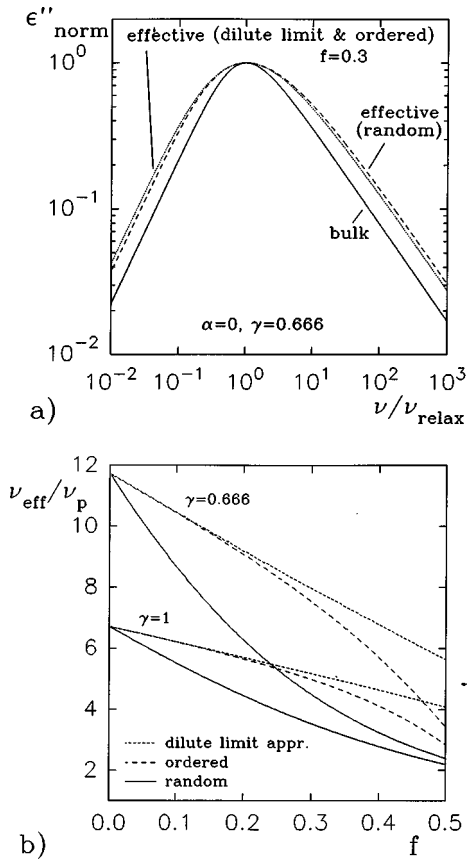

FIG. 4. (a) Normalized imaginary part of the permittivity $\varepsilon''/\varepsilon''_{\max}$ for an asymmetric bulk relaxation [Eq. (19) with parameters as in Fig. 3 but with $\gamma=0.666$] and for the effective relaxation of dispersed droplets ($f=30\%$). The frequency axis is normalized to the respective relaxation frequency $\nu_{\rm relax}=\nu_p$ or $\nu_{\rm relax}=\nu_{\rm eff}$. (b) Frequency shift $\nu_{\rm eff}/\nu_p$ vs filling factor for a symmetric relaxation where $\gamma=1$ [values of Fig. 3(c)] and for the asymmetric case with $\gamma=0.666$. Dilute limit approximation: Eq. (3); ordered: Eq. (12) for the simple cubic lattice; random: Hanai-Bruggeman Eq. (13).

$$\frac{\varepsilon''_{\rm eff}}{\Delta\varepsilon_{\rm eff}}(\nu\ll\nu_{\rm eff})\simeq\sin[(1-\alpha)\pi/2]\gamma\left(\frac{\nu}{\nu_0 F}\right)^{1-\alpha}, \quad (24)$$

$$\frac{\varepsilon''_{\rm eff}}{\Delta\varepsilon_{\rm eff}}(\nu\gg\nu_{\rm eff})\simeq\sin[(1-\alpha)\pi/2]\left(\frac{\nu_0 F^{1/\gamma}}{\nu}\right)^{(1-\alpha)\gamma}. \quad (25)$$

A comparison with Eqs. (20) and (21) reveals that the low frequency side is shifted to higher frequencies by a factor of F (as for symmetric peaks), while the high frequency side is shifted by $F^{1/\gamma}$. Since $F^{1/\gamma}>F$ for $\gamma<1$, the effective loss peak is broadened compared to that of the intrinsic particle permittivity, but the respective slopes of the low and of the high frequency side are unchanged. This effect is shown in Fig. 4(a). According to the above analysis, the shift of the relaxation frequency can be estimated to be

$$\frac{\nu_{\rm eff}}{\nu_p}\simeq\frac{F^{1/\gamma}+F}{2}, \quad (26)$$

with F from Eq. (7) or (16), respectively (dilute limit or random). This reduces to the correct result $\nu_{\rm eff}/\nu_p=F$ in the symmetric case. Exact values of a numerical analysis [inserting Eq. (19) in Eqs. (3), (12), and (13)] are displayed in Fig. 4(b). The shift of the relaxation frequency increases with increasing asymmetry ($\gamma<1$) of the intrinsic relaxation. As in the symmetric case ($\gamma=1$), it decreases with increasing interaction, i.e., with increasing disorder or filling factor. Summarizing, the asymmetry of the intrinsic relaxation shifts the effective relaxation to higher frequencies and alters its shape.

D. Experimental results

In this section we discuss experimental data[8–10,39] on the so-called α relaxation of propylene glycol (PG). The confining matrix is butyl rubber with $\varepsilon_m=2.3$, a material that has been used to study nanometer droplets of water as well as of various glass forming liquids.[8–11,40] The sample preparation is described in Ref. 40. The rubber is immersed in a liquid at constant temperature and pressure. Droplets form at absorption sites via a molecular diffusion process.[40] There are no voids in the matrix, but the droplets arise against the counter pressure of the elastic rubber and are therefore of spherical shape. A reduced density due to a difficulty in packing the molecules seems unlikely. The size distributions of the droplets were determined by means of small angle x-ray scattering using the structure-interference method.[41] The mean diameter increases with increasing filling factor. In the case of PG, for example, from $d=7.2$ nm at $f=0.028$ to $d=10.2$ nm at $f=0.164$.[39] The half width of the respective size distribution is about $d/3$. Both the spatial distribution of the absorption sites and the droplet size distribution result in a distribution of the interparticle spacing and thus a random system is obtained. The dielectric data was obtained by means of a transmission technique that allows for frequency- and temperature-dependent calibration.[42] These single-sweep measurements on one sample holder cover the entire frequency range from 5 Hz to 2 GHz.

Figure 2 displays the permittivity of the bulk liquid at 218 K. The asymmetric peak of the α relaxation is located at 274 kHz. It shifts to lower frequencies when the temperature is lowered (see Refs. 8,10). The effective values for PG confined in rubber are much smaller and the α relaxation appears at higher frequencies (the additional low frequency peak is discussed in Refs. 8–10). Figure 5(a) displays the relaxation strength of the α process for bulk PG. While $\varepsilon_{p,\infty}\simeq 3$, $\Delta\varepsilon_p$ depends on temperature. A fit yields $\Delta\varepsilon_p\simeq -25+14300/(T[\mathrm{K}])$. We also show the effective relaxation strength for PG nanodroplets in rubber with $f=0.164$. $\Delta\varepsilon_{\rm eff}$ is much weaker than the intrinsic bulk values and independent of temperature. This effect is expected in the limit of strongly polar materials, where $\Delta\varepsilon_{\rm eff}$ becomes independent of the intrinsic relaxation process and is only a function of filling factor, microstructure, and matrix permittivity [Eqs. (11) and (18)]. The experimental data is compared to effective medium calculations using the bulk permittivity of PG. Obviously, the effective relaxation strength is well described by Eq. (13) which applies for a random spatial distribution of droplets. The dilute limit approximation predicts too small values. Figure 5(b) shows that the spatial distribution of the droplets becomes important with increasing filling factor. Above $f=0.1$ a deviation from the dilute limit approximation becomes visible and the variation of the experimental data increases.

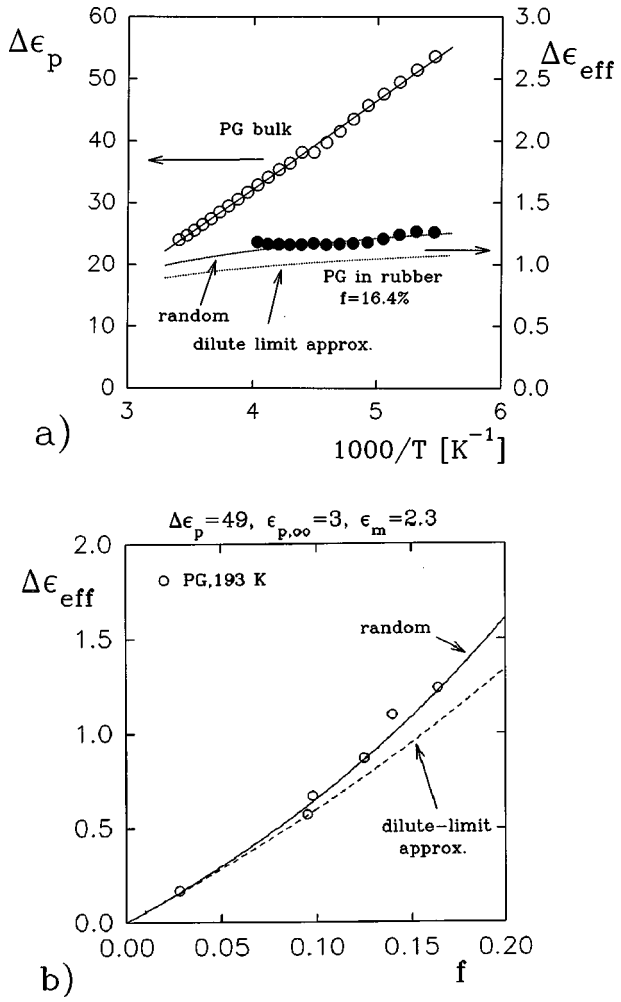

FIG. 5. (a) Relaxation strength vs reciprocal temperature for the α relaxation of bulk PG (left y axis) and of PG in butyl rubber (right y axis). Symbols: experiment; dotted lines: calculations (no fit) according to Eqs. (8) and (13), i.e., the dilute limit approximation and the Hanai-Bruggeman result for random sytems, respectively. (b) Relaxation strength vs filling factor (symbols) for PG confined in rubber at 193 K compared with calculations (lines).

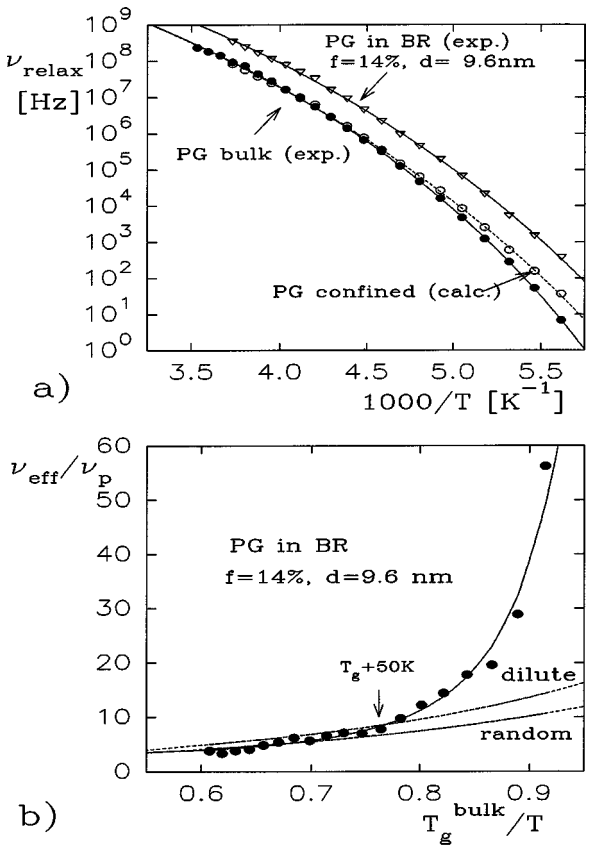

FIG. 6. (a) Relaxation frequency of the α process vs $1/T$ for bulk PG (filled circles, ν_p) and for an effective PG-rubber system (open triangles, $\nu_{\rm eff}$). The values for the confined liquid (open circles, $\nu_{\rm conf}$) are obtained via an effective medium correction (see text). Obviously, $\nu_{\rm conf}\simeq\nu_p$ at high temperatures, but $\nu_{\rm conf}>\nu_p$ at low temperatures. (b) Frequency shift $\nu_{\rm eff}/\nu_p$ vs T_g/T at $f=0.14$. Symbols: experiment; solid line: fit; dashed lines: calculation according to the dilute limit approximation, Eq. (3), and to (13) (random system) using the bulk values for PG.

Now let us discuss the temperature dependence of the relaxation frequency, which obeys the Vogel-Fulcher-Tamman law

$$\log_{10}(\nu_p)=\log_{10}A-\frac{B}{T-T_0} \tag{27}$$

[see filled circles in Fig. 6(a)]. For the bulk liquid $A\simeq 2\times10^{13}$ Hz, $B\simeq840.7$ K, and $T_0\simeq110.7$ K holds.[10] An extrapolation of Eq. (27) to $\nu_p(T_g)=1/628$ Hz [$\tau_p(T_g)=100$ s, see Ref. 3] yields the dielectric glass transition temperature $T_g^{\rm bulk}\simeq162.8$ K. The effective relaxation frequencies of the confined liquid are enhanced compared to those of the bulk liquid [open triangles and filled circles in Fig. 6(a)]. As we have shown above, the frequency shift $\nu_{\rm eff}/\nu_p$ depends on the shape parameters of the bulk process. A fit of the experimental data for PG (see Ref. 10, Fig. 9) yields $\alpha\simeq0$ and $\gamma\simeq1.1-81.4/(T[\mathrm{K}])$, i.e., broadening and asymmetry increase with decreasing temperature. In Fig. 6(b) the observed frequency shift for a filling factor of $f=0.14$, i.e., for a mean droplet diameter of $d=9.6$ nm, is compared with effective medium calculations. For this purpose a numerical analysis of the dilute limit approximation, Eq. (3), and of the Hanai-Bruggeman result, Eq. (13), has been carried out using the bulk values for PG. Since relaxation strength [Fig. 5(a)] and asymmetry of the bulk relaxation increase with decreasing temperature, the calculated $\nu_{\rm eff}/\nu_p$ values increase [see, e.g., Eqs. (7), (16), and (26)]. At first, we focus on temperatures far above the glass transition, $T\geqslant T_g+50$ K ($T\geqslant1.3T_g$): the observed shift is in agreement with the theory for random systems while the dilute limit approximation yields too high values. Obviously, the shift of the effective relaxation frequency is only due to dielectric heterogeneity of the PG-rubber system, i.e., an effective medium effect. This result, as well as the fact that the droplets form against the counter pressure of the rubber, allows us to rule out a markably reduced density of the confined liquid, which should give rise to an additional increase of the relaxation frequency. The finite volume does not seem to induce structural changes that affect ν_p. Also surface effects are not observed. Enforced bonds at a large internal surface can result in a decrease of the relaxation frequency.[6,19] But the hydrophobic rubber does not interact

with PG, a hydrogen bonded liquid. Only hydrophilic impurities of the rubber matrix can retard the dynamics of some PG molecules, which relax at much lower frequencies and do not contribute the α-process of the inner mobile sphere.[8–10] Obviously, the interaction with these slow surface molecules is sufficiently weak not to affect the mean relaxation frequency of the bulklike molecules inside the droplets.

Approaching T_g the experimental frequency shift is higher than that predicted by the effective medium theory [see Fig. 6(b)]. Figure 6(a) compares the relaxation frequencies of bulk PG, of the effective PG-rubber system, as well as of the confined liquid. Care has to be taken in the evaluation of the latter ones: as we shall see below, surface effects alter the shape of the relaxation, an effect that effective medium formulas for dielectrically homogeneous particles cannot take into account. Inverting Eq. (13), i.e., inserting the measured $\varepsilon_{\rm eff}$ and solving for $\varepsilon_p^{\rm conf}$, would not yield correct results, since shape and frequency shift are related. Here, the relaxation frequencies of the confined droplets have been obtained dividing the measured effective frequencies by the above calculated frequency shift that is expected in the absence of size or surface effects [using Eq. (13) and the bulk values of ε_p, see Fig. 6(b)]. At low temperatures the confined molecules relax faster than those of the bulk liquid. This is equivalent to a decrease of the glass transition temperature T_g. For the confined liquid a fit according to Eq. (27) yields $T_g^{\rm conf}=157$ K, so that $T_g^{\rm conf}=T_g^{\rm bulk}-5.8$ K. The smaller the droplets are, the stronger the effect becomes.[8–10] The lowering of T_g is displayed in Fig. 7 [the errors are mainly due to the low-frequency extrapolation of Eq. (27)]. The finite-size effect vanishes at an extrapolated radius of 5-6 nm, which has been associated with the cooperativity length, i.e., with an intrinsic nanoscale heterogeneity in PG.[8–11]

Finally, we investigate the shape of the α process for $T \geqslant T_g+50$ K, where the above finite-size effect is not yet effective (Fig. 8). The experimental data for the bulk permittivity was used to calculate the effective response that is expected in the absence of confinement or surface effects. In this temperature range the Hanai-Bruggeman formula, Eq. (13), describes fairly well both the relaxation strength and the relaxation frequency of the effective PG-rubber system. It predicts a broadening of the α relaxation, but it fails to describe the observed shape. The experimental data shows an even broader peak and also the respective low and high frequency slopes differ. Obviously, dielectric heterogeneity of the effective medium contributes to the effective half width, but there is an additional effect. Nonuniformity of interactions is known to cause a distribution of relaxation frequencies and thus a broadening.[25,26] As in the bulk liquid, the majority of PG molecules in the center of the confined volume only interact with surrounding molecules of the same type via fluctuating hydrogen bonds. These molecules determine the intrinsic relaxation frequency ν_p (see above). At the surface of the hydrophobic rubber walls there are less hydrogen bonds so that the reorientation becomes faster, while it is retarded in the vicinity of less mobile PG molecules bonded to hydrophilic impurities of the rubber matrix (even though the bonded molecules do not contribute to the α relaxation of the inner mobile sphere[8–10]). The superposition of different relaxation frequencies results in a broadening of the peak. Its

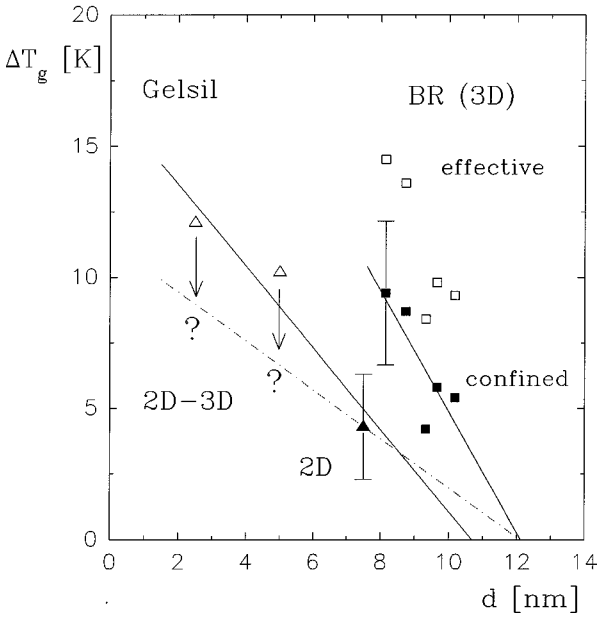

FIG. 7. Lowering of the glass transition temperature $\Delta T_g = T_g^{\rm bulk} - T_g^{\rm conf}$ vs droplet or pore diameter for 3D confined droplets of PG and for 2D-3D confined pores. For the 3D case both the effective values (open squares) and the values for the confined liquid (filled squares) are displayed. The latter ones are about 4–5 K smaller and were obtained from an effective medium analysis according to Eq. (13). For the pores only effective values are shown. At $d=7.5$ nm there is a true 2D confinement, so that the effective temperature shift equals that of the confined liqid. The 2D-3D topology at lower pore sizes would require an effective medium correction. Its magnitude should not be larger than for the 3D case, but the exact values are unknown. As indicated by the arrows and the dashed line, even a shift of 3 K would not markedly affect the extrapolated diameter, at which the finite-size effect vanishes.

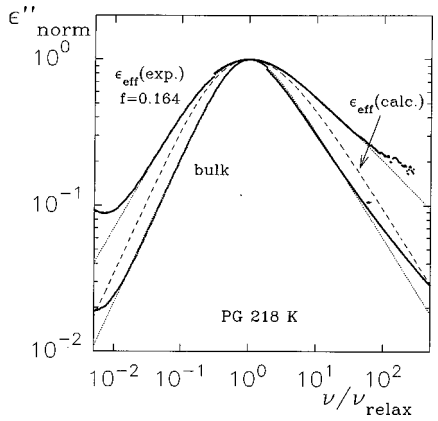

FIG. 8. Normalized α relaxation $\varepsilon''/\varepsilon''_{\rm max}$ of bulk PG and PG confined in rubber ($f=16.4\%$) at $T=218$ K, i.e., 55.2 K above the glass transition temperature of the bulk liquid. The frequency axis is normalized to the respective relaxation frequency, $\nu_{\rm relax}=\nu_p$ or $\nu_{\rm relax}=\nu_{\rm eff}$. The dotted lines are fits of the experimental data to the Havrilak-Negami formula [Eq. (19)]. The dashed line is an effective medium calculation using the bulk values [Hanai-Bruggeman formula, Eq. (13)]. As expected the calculated peak is much broader than the bulk response, and not of the Havrilak-Negami form. The deviation between calculated and measured effective response is due to a surface effect (see text).

half width is constant for $T>T_g+50$ K; below it increases with decreasing temperature (Ref. 10, Fig. 9). Therefore, in the vicinity of T_g a third effect might contribute to the broadening, e.g., an intrinsic nanoscale heterogeneity of PG.[10]

Summarizing, the effective relaxation strength is well described by the Hanai-Bruggeman effective medium theory for random systems. It is even possible to resolve the deviations from the dilute limit approximation. The same holds for the effective relaxation frequency at high temperatures $T>T_g+50$ K. There are no density, surface, or confinement effects, that are strong enough to alter the relaxation frequency or relaxation strength. Approaching T_g a finite-size effect is observed: the molecular relaxation becomes faster compared to bulk. Details of the surface roughness and interaction seem to affect only the shape of the effective relaxation. Already at high temperatures a broadening is observed which is partly due to dielectric heterogeneity of the effective medium and partly due to a surface effect. We conclude that in systems of 3D confined droplets finite-size and surface effects can be reliably and quantitatively extracted from dielectric data.

II. 2D CONFINEMENT

Confining a material in two dimensions yields one-dimensional channel-like structures [see Fig. 1(c)]. Here the term ''2D confinement'' only refers to continuous pores running right through the whole sample, since otherwise also the third dimension would be partially confined [see Fig. 1(b)]. For the same reason the pore surfaces have to be sufficiently smooth and nonfractal. Of course, the surrounding matrix extends in three dimensions and therefore the effective medium analysis remains a 3D problem. As we have seen above, the calculation of the effective permittivity requires the detailed information on the microstructure, e.g., in the form of local porosity distributions.[44,45] For most real systems, such as porous glasses, this information is not available for the time being. For this reason we first discuss two simple random pore topologies. This will allow us to determine some characteristic properties of 2D-confined materials and to decide, which part of the dielectric data can be used to get reliable information on confinement effects. Later we shall focus on the problem of to what extent can the topology of real systems be regarded as 2D in the sense of an effective medium approach [see the dead ends of the pores in Fig. 1(b)].

A. Noncrossing straight pores

Noncrossing straight pores filled with a material can be considered as the limiting case of prolate spheroids of infinite length. When these rodlike inclusions are orientated in the direction of the applied field the depolarization factor is $A=0$, while it is $A=1/2$ for a perpendicular orientation. Only in the latter case there is a phase shift between the mean fields in matrix and filler resulting in an increased effective relaxation frequency [see Eqs. (5), (7), and (26)]. For a random orientation at very low f the effective permittivity is obtained by the superposition of three orientations: $\varepsilon_{\rm eff}=1/3\varepsilon_{\rm eff}^{A=0}+2/3\varepsilon_{\rm eff}^{A=0.5}$ [see Eq. (3)]. Neglecting the term fx in the denominator of Eq. (3) Fricke obtained a dilute limit approximation[29]

$$\varepsilon_{\rm eff}=\varepsilon_m\left(1+\frac{f}{3}\sum_{i=1}^{3}\frac{\varepsilon_p-\varepsilon_m}{\varepsilon_m+A_i(\varepsilon_p-\varepsilon_m)}\right)$$
$$=1+\frac{f}{3}(\varepsilon_p-\varepsilon_m)+\frac{4f}{3}\varepsilon_m\frac{1-\varepsilon_m/\varepsilon_p}{1+\varepsilon_m/\varepsilon_p}\quad\text{for } f<0.1. \tag{28}$$

The second term $\propto\varepsilon_p$ corresponds to the relaxation of the parallel component that is located at the relaxation frequency of the filler ν_p. The last term is due to the pores perpendicular to the field. They give rise to a second relaxation process. Figure 9(a) displays the permittivity according to Eq. (28) for a large relaxation strength. The parallel component dominates and there is no shift of the effective relaxation peak, a result that does not depend on the filling factor or on the shape of the intrinsic relaxation [Eqs. (2) and (19)]. The $A=1/2$ component becomes visible at the high frequency side of the main loss peak but with a much smaller amplitude. But

$$\nu_{\rm eff}\simeq\nu_p \tag{29}$$

holds also in the limit of small relaxation strengths, where both relaxations coincide at ν_p [$F_{A=0.5}\to 1$, see Eq. (7)]. For the effective relaxation strength $\varepsilon_{\rm eff}(\varepsilon_p=\Delta\varepsilon_p+\varepsilon_{p,\infty})-\varepsilon_{\rm eff}(\varepsilon_p=\varepsilon_{p,\infty})$, Eq. (28) yields

$$\Delta\varepsilon_{\rm eff}\simeq\frac{f}{3}\left[\Delta\varepsilon_p+\frac{8\varepsilon_m}{1+\varepsilon_{p,\infty}/\varepsilon_m}\right]\quad\text{for } \Delta\varepsilon_p+\varepsilon_{p,\infty}\gg\varepsilon_m, \tag{30}$$

where the first term is due to the parallel component. Thus, $\Delta\varepsilon_{\rm eff}\propto\Delta\varepsilon_p$ in contrast to 3D-confined droplets, where the effective relaxation strength of strongly polar materials becomes independent of the intrinsic relaxation process [see Eqs. (11) and (18)]. Although Eq. (28) is a dilute limit approximation, it serves to illustrate that the pores in the direction of the field and thus the properties of the filler dominate the response. These can only emerge more clearly at higher filling factors and the results $\nu_{\rm eff}\simeq\nu_p$ and $\Delta\varepsilon_{\rm eff}\propto\Delta\varepsilon_p$ should remain valid.

As in the case of spheres, particle interaction at higher filling factors can be taken into account via an integration method. Starting from Eq. (28) Niesel obtained a formula for randomly orientated rods[29,46]

$$\frac{\varepsilon_{\rm eff}-\varepsilon_p}{\varepsilon_m-\varepsilon_p}\left(\frac{5\varepsilon_m+\varepsilon_p}{5\varepsilon_{\rm eff}+\varepsilon_p}\right)^{2/5}=1-f\quad\text{for } f<f_c, \tag{31}$$

that is the analogue of the Hanai-Bruggeman result for spheres, Eq. (13). Once again, the mean field approximation is expected to fail when the dispersed rods are close together, at the latest for $f\geqslant 0.5$. The permittivity is displayed in Fig. 9(a). Particle interaction leads to higher permittivities compared with the dilute limit approximation Eq. (28), but the peak frequency remains unchanged [see Figs. 9(b) and 9(c)]. While the two components of the relaxation are clearly visible in the dilute limit approximation, they unify according to Eq. (31) and only a weak shoulder remains visible at the high frequency side of the peak [Fig. 9(a)]. Figure 10 shows that compared to the bulk relaxation only the slope on the high frequency side is altered. Fitting the Havriliak-Negami for-

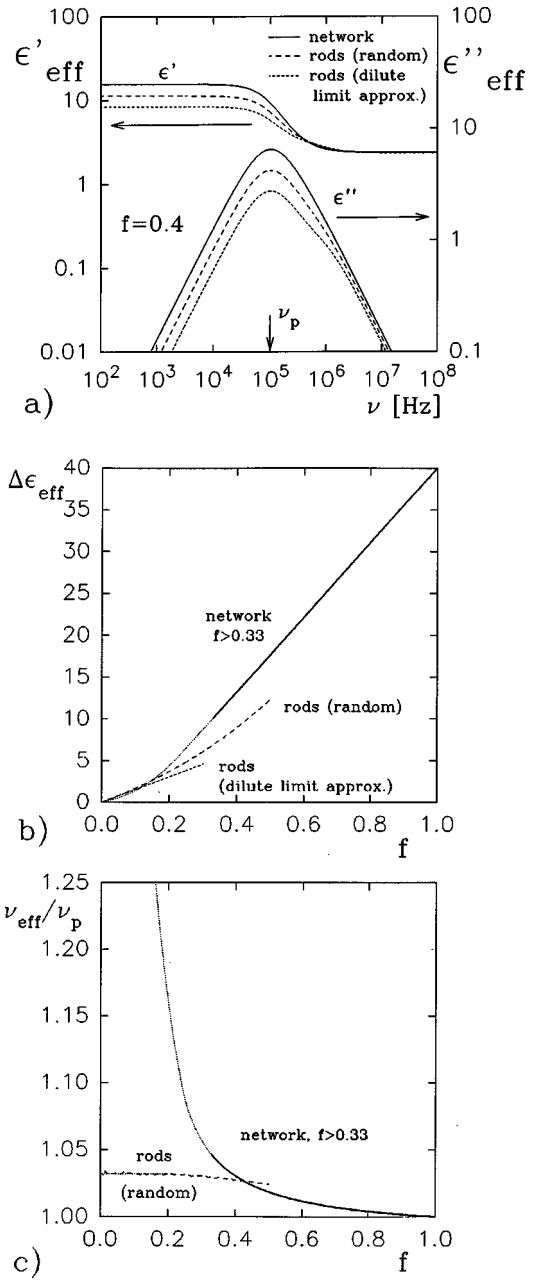

FIG. 9. Relaxation process for 2D-confined material with $\Delta\varepsilon_p = 40$, $\varepsilon_{p,\infty} = 3$, $\nu_p = 10^5$ Hz, $\alpha = 0$, $\gamma = 1$, and $\varepsilon_m = 2$. (a) Effective permittivity vs frequency at filling factor 40%. (b) Relaxation strength and (c) frequency shift $\nu_{\rm eff}/\nu_p$ vs filling factor. Rods: randomly orientated noncrossing pores; dilute limit approximation Eq. (28) and Niesel formula Eq. (31); network of interconnected pores: Stölzle formula, Eq. (38), for the aggregate topology [see Fig. 1(c)].

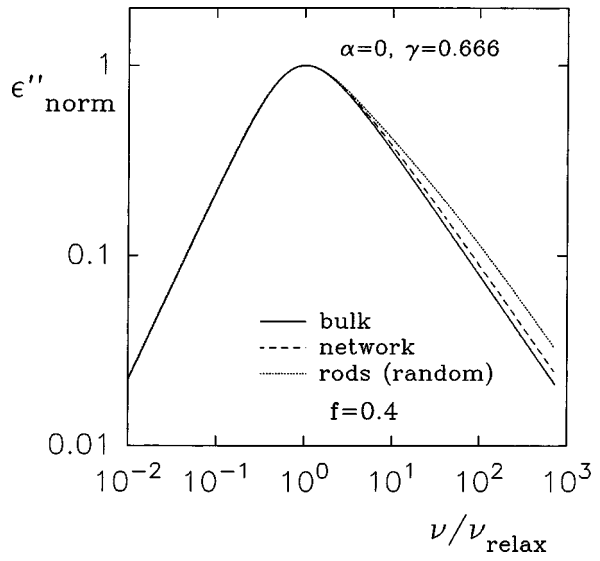

FIG. 10. Imaginary part of the normalized permittivity $\varepsilon''/\varepsilon''_{\rm max}$ vs normalized frequency ($\nu_{\rm relax} = \nu_p$ or $\nu_{\rm relax} = \nu_{\rm eff}$, respectively) for an asymmetric bulk relaxation as well as for an effective system of noncrossing rods and for a network of interconnected pores ($f = 40\%$). Apart from the shape parameters $\alpha = 0$ and $\gamma = 0.666$, all other material parameters are as in Fig. 9. Bulk: Eq. (19); rods: Eq. (31); network: Eq. (38).

mula [Eq. (19)] to the effective permittivity would yield the α value of the bulk material but a smaller effective γ.

Once again, let us consider the limit of strongly polar materials $|\varepsilon_p| \gg \varepsilon_{p,\infty} \gg \varepsilon_m$ and sufficiently low filling factors, so that $|\varepsilon_p| \gg |\varepsilon_{\rm eff}|$. In this limit Eq. (31) becomes

$$(1-f)^{5/2}\frac{5\varepsilon_{\rm eff}+\varepsilon_p}{5\varepsilon_m+\varepsilon_p} = \left(\frac{1-\varepsilon_{\rm eff}/\varepsilon_p}{1-\varepsilon_m/\varepsilon_p}\right)^{5/2} \tag{32}$$

$$\simeq 1 - \frac{5}{2}\frac{\varepsilon_{\rm eff}}{\varepsilon_p} + \frac{5}{2}\frac{\varepsilon_m}{\varepsilon_p} + \cdots \tag{33}$$

and thus

$$\varepsilon_{\rm eff} \simeq \varepsilon_m \frac{3+5\varepsilon_m/\varepsilon_p}{1+2(1-f)^{5/2}+5\varepsilon_m/\varepsilon_p} + \frac{2}{5}\varepsilon_p \frac{1-(1-f)^{5/2}}{1+2(1-f)^{5/2}+5\varepsilon_m/\varepsilon_p}. \tag{34}$$

Since $|\varepsilon_m/\varepsilon_p| \ll 1$, the term $\propto \varepsilon_p$ and thus the pores in the direction of the applied field dominate the frequency dependence of $\varepsilon_{\rm eff}$. Inserting Eq. (2) or Eq. (19) yields

$$\nu_{\rm eff} \simeq \nu_p, \tag{35}$$

$$\Delta\varepsilon_{\rm eff} \simeq \frac{2}{5}\frac{1-(1-f)^{5/2}}{1+2(1-f)^{5/2}}\Delta\varepsilon_p \quad \text{for } \varepsilon_{p,\infty} \gg 5\varepsilon_m. \tag{36}$$

As in the dilute limit $\nu_{\rm eff} \simeq \nu_p$ and $\Delta\varepsilon_{\rm eff} \propto \Delta\varepsilon_p$ hold. Figure 11 shows that the validity of these relations is not restricted to the case $\varepsilon_{p,\infty} \gg \varepsilon_m$.

Of course, the above analysis is not based on an explicit calculation of higher multipole moments. But we can conclude that for a random 2D confinement of noncrossing pores the channels with an orientation parallel to the field dominate the response. The effective relaxation strength increases linearly with $\Delta\varepsilon_p$ and the relaxation frequency is more or less that of the bulk relaxation, no matter whether it is symmetric or asymmetric. This result does not depend on the values of f and $\Delta\varepsilon_p$ [see Figs. 9(c) and 11]. The shape of the bulk relaxation is preserved on the low frequency side of the peak.

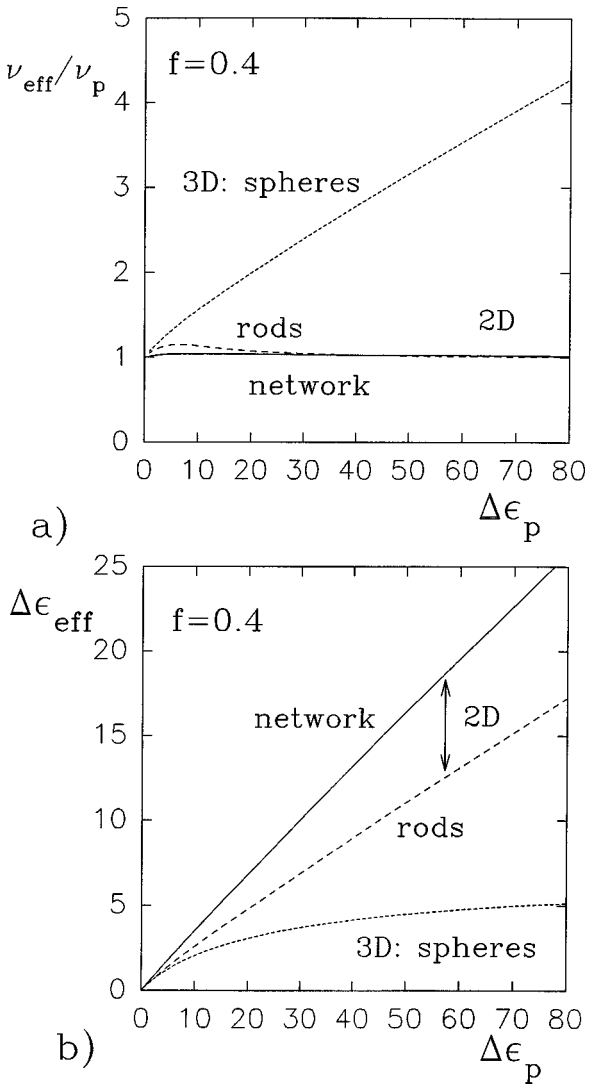

FIG. 11. (a) Frequency shift $\nu_{\rm eff}/\nu_p$ and (b) effective relaxation strength vs intrinsic relaxation strength for 2D- and 3D-confined materials at $f=0.4$ according to a numerical analysis of Eq. (13) (spheres), Eq. (31) (rods), and Eq. (38) (network). For the material parameters see the caption of Fig. 9.

But on the high frequency side the pores perpendicular to the field become noticable causing a flatter response and thus a small broadening.

B. Network of interconnected pores

In all previous sections we have considered the matrix inclusion topology, where spatially separated spheres or rods (the filler) are surrounded by a continuous phase (the matrix), all regions of which are perfectly interconnected. This topology is not suited for systems, where also the filler phase exhibits a high degree of interconnection between its dispersed elements [see Fig. 1(c)]. Although one might imagine a channel-like structure assembled of agglomerating particles, the description of such a nonrandom disordered system would be rather complicated. For an approximative description it is more convenient to use the so-called ''aggregate topology,'' where two topologically equivalent phases are randomly mixed.[21] *Inter alia* it is appropriate for compact powders, heterogeneous polymer mixtures, and interpenetrating network structures.[28] For example, also the local porosity formalism[44,45] starts from a symmetric effective medium formula, which characterizes an aggregate topology. Figure 1(c) shows a sketch of a microstructure, where matrix and filler are randomly distributed on a cubic grid. Above the critical filling factor $f_c=0.33$, where continuous paths of the filler material form, both matrix and filler phase are interconnected. Note that seemingly isolated segments are for the most part connected via the layers behind or in front of the displayed cross section. We do not discuss the variety of approximative mean field formulas,[29,30] since we are considering high filling factors $f_c<f<1$ and fillers with large permittivities, so that multipole fields have to be taken into account. For the above cubic-grid structure precise numerical simulations including all higher multipole moments have been performed.[47,48] The results for $|\varepsilon_p|\leqslant 100$ are well described (with an accuracy of 3%) by

$$\varepsilon_{\rm eff}(f)=[(1-f)\varepsilon_m^a+f\varepsilon_p^a]^{1/a} \quad \text{for } f\leqslant 0.25, \tag{37}$$

$$\varepsilon_{\rm eff}(f)=\frac{1}{0.75}\{(1-f)\varepsilon_{\rm eff}(0.25)+(f-0.25)\varepsilon_p\} \quad \text{for } f\geqslant 0.25, \tag{38}$$

where

$$a=1.6f+0.265.$$

Here we are only interested in the range $f>f_c=0.33$, where the aggregate topology corresponds to a 2D confinement. Figure 9(a) compares the permittivity spectrum for the above aggregate topology with that for a system of noncrossing pores. Equation (38) yields higher permittivity values for both the real and the imaginary part. However, the peak position is that of the bulk relaxation. It is obvious, that for $f>f_c$ the second term $\propto f\varepsilon_p$ dominates in Eq. (38) and thus

$$\nu_{\rm eff}\simeq\nu_p, \tag{39}$$

$$\Delta\varepsilon_{\rm eff}\propto f\Delta\varepsilon_p. \tag{40}$$

Figures 9(c) and 11(a) display the exact frequency shift $\nu_{\rm eff}/\nu_p$. It is close to 1 for filling factors above $f_c=0.33$, where the first continuous paths form. Figures 9(b) and 11(b) show that the relaxation strength increases linearly with both filling factor and relaxation strength.

Summarizing, paths or parts of paths parallel to the applied field govern the response. Compared to systems of noncrossing straight pores, the interconnection reinforces the dominance of the parallel component: the frequency shift is even closer to 1 [Fig. 9(c)], the relaxation strength is larger [Fig. 9(b)], and the form of the effective relaxation can be hardly distinguished from that of the bulk material (Fig. 10).

C. Real porous systems

As we have seen above, the values of $\varepsilon_{\rm eff}$ depend on details of the pore topology, *inter alia* on the curvature and on the degree of interconnection [see Figs. 1(c) and 9(a),9(b)]. A general characterization of dielectric heterogeneity in a random 2D confinement of continuous pores is

nevertheless possible. The basic features arise out of the dominance of the parallel components and contrast with those of 3D confinements:

(i) The effective relaxation strength increases linearly with $\Delta\varepsilon_p$, at least for large values:

$$\Delta\varepsilon_{\text{eff}} \simeq a\Delta\varepsilon_p + b, \tag{41}$$

where a and b depend on f, ε_m, $\varepsilon_{p,\infty}$, and on the microstructure [see Fig. 11 and Eqs. (30),(36),(40)]. $0<a<1$ holds since $\Delta\varepsilon_{\text{eff}}<\Delta\varepsilon_p$ for $f<1$. Therefore, the temperature dependence of $\Delta\varepsilon_{\text{eff}}$ is weaker than that of $\Delta\varepsilon_p$. Remember that for 3D-confined droplets smaller values are obtained and $\Delta\varepsilon_{\text{eff}}$ becomes independent of the intrinsic relaxation process in the limit of large $\Delta\varepsilon_p$ [see Fig. 11 and Eqs. (11),(18)].

(ii) The effective relaxation frequency roughly equals that of the filler material

$$\frac{\nu_{\text{eff}}}{\nu_p} \simeq 1 \tag{42}$$

[see Figs. 9(c), 11, and Eqs. (29),(35),(39)].

(iii) The shape of the relaxation is preserved on the low frequency side of the peak, while it is only weakly modified on the high frequency side (see Fig. 10).

The above characteristics should be observable as long as no size or surface effects give rise to deviations. Vice versa, they allow us to control whether a given microstructure corresponds to a random 2D confinement. This is of practical importance, since controlled porous glasses (CPG's) are often used in confinement experiments, although only little is known about their exact topology. Small-angle neutron or x-ray scattering revealed fractally rough interfaces.[1,49,50] In Vycor glass (Corning 7930) the fractal dimension of the pore surfaces is about 2.5 (Ref. 49), while in various silica gels values of 2.15 were found.[50] Whatever the exact microstructure is, the deciding factor is the partial confinement of the third dimension. Figure 1(b) shows a system in which a large part of the material is confined in pores that do not run right through the whole sample. The dead ends act as an intermediate state between channels and droplets. The system exhibits an intermediate 2D-3D topology and the parallel components are no longer expected to govern the dielectric response.

In the following we discuss experimental data on bulk propylene glycol (PG) and on PG in controlled porous Gelsil glasses.[8–10,39] The glasses exhibit nominal porosities of $p=48$, 63, and 70 % that correspond to pore diameters of 2.5, 5.0, and 7.5 nm. It should be noted that p equals f only when a complete filling is achieved. But the above features (i)–(iii) can be checked experimentally even when the exact filling factor or the matrix permittivity are unknown [measuring the permittivity of the unfilled glass yields $\varepsilon_{\text{eff}}(\varepsilon_p=1,\varepsilon_m)$, but the calculation of ε_m requires a detailed knowledge of the microstructure]. Figure 2 displays some permittivity spectra at 218 K. The labels for the dimensionsalities are anticipated but will become comprehensible in the following.

Figure 12 displays the effective relaxation strengths vs that of bulk PG [see Fig. 5(a)]. For the highest porosity and pore diameter the linear relation Eq. (41) holds. When the temperature is lowered, $\Delta\varepsilon_p$ increases and so does $\Delta\varepsilon_{\text{eff}}$. As expected, its temperature dependence is less strong, so that the slope is $a<1$. But at lower porosities much smaller $\Delta\varepsilon_{\text{eff}}$ values are observed, which are independent of temperature or of $\Delta\varepsilon_p$. This behavior calls to mind 3D confinements [Fig. 5(a) and 11(b)], although there are continuous pores across the samples (these manifest via an effective dc conductivity that is due to ionic impurities of PG). Therefore, Fig. 12 gives a first hint to a gradual change of topology from 2D at high porosity and pore diameter to an intermediate 2D-3D topology at low porosities (see below).

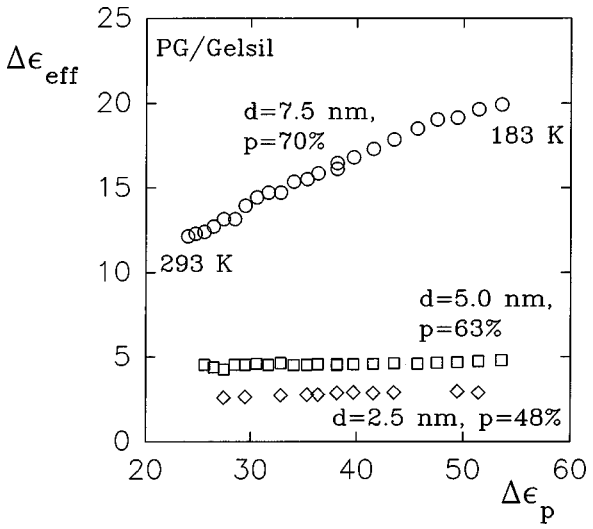

FIG. 12. Effective relaxation strength vs relaxation strength of the bulk liquid for the α relaxation of propylene glycol in porous Gelsil glasses of different porosities and pore sizes: 48% ($d=2.5$ nm), 63% ($d=5$ nm), 70% ($d=7.5$ nm). Data in the temperature range from 183–293 K (see Fig. 5).

The temperature dependence of the relaxation frequencies follows the Vogel-Fulcher-Tamman law, Eq. (27), and is similar to that displayed in Fig. 6(a) for the 3D-confined droplets (see also Ref. 8, Fig. 2). Figure 13 shows the frequency shift of the effective relaxation frequency. At first we

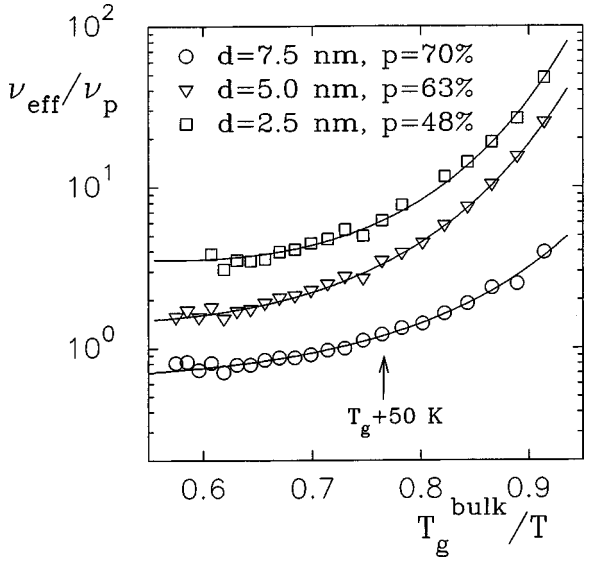

FIG. 13. Frequency shift ν_{eff}/ν_p vs glass transition temperature over temperature T_g^{bulk}/T for the α relaxation of PG confined in porous Gelsil glass (see Fig. 12).

focus on temperatures far above the glass transition $T > T_g + 50$ K where we do not expect any size effects, so that ν_{eff}/ν_p is a figure of merit characterizing the topology. The largest pores ($d = 7.5$ nm, 70% porosity) show the expected 2D result $\nu_p \simeq \nu_{\mathrm{eff}}$. Strictly speaking, ν_{eff} is slightly smaller than ν_p, but this small deviation might be due to an interaction with a retarded layer of directly surface attached molecules, even if the latter ones do not contribute to the α process of the bulklike molecules in the center of the pores.[6,8–10,18] However, the high-temperature limit of the frequency shift ν_{eff}/ν_p increases from $\nu_{\mathrm{eff}}/\nu_p \simeq 0.8$ at 70% to $\nu_{\mathrm{eff}}/\nu_p \simeq 1.8$ at 63% and finally $\nu_{\mathrm{eff}}/\nu_p \simeq 3.5$ at 48%. A faster molecular reorientation due to a reduced density of the confined liquid is improbable: although it would explain the increase of ν_{eff} with decreasing pore size, it is inconsistent with the supression of the temperature dependence of $\Delta\varepsilon_{\mathrm{eff}}$ at low porosities (Fig. 12). A possible reduction of density as a result of difficulty in packing the molecules has been briefly mentioned in the literature, but the authors have rejected the idea *inter alia* because of the pressure dependence of the glass transition temperature.[4] On the other hand, a gradual change of topology from 2D at the high porosity and pore diameter to an intermediate 2D-3D topology at low porosities explains both the behavior of $\Delta\varepsilon_{\mathrm{eff}}$ (see above) and the increasing high temperature limit of the relaxation frequency. At the highest porosity, $p = 70\%$, most of the space is occupied by the liquid and so there is high amount of continuous pores which dominate the response. At lower porosities there is enough matrix material to form voids or dead ends [see Fig. 1(b)]. But also a variation of the pore size might prevent a complete filling and result in a similar structure. The hypothesis of a topological change can be tested, since the value of the frequency shift depends not only on the microstructure of the Gelsil glasses but also on the relaxation strength of the filler [see Fig. 11 and Eqs. (16) and (26) for pure 3D confinement]. The smaller $\Delta\varepsilon_p$ is, the less pronounced the effect should be. In fact, it is observable for PG, where $\Delta\varepsilon_p \simeq 24$ at room temperature. But it does not appear for Salol (Ref. 6, Fig. 3), the relaxation strength of which is about six times smaller.[51] Even if it is easier to analyze data of less polar liquids, where dielectric heterogeneity does not affect ν_p, information on the microstructure of the confinement can only be obtained from measurements of strongly polar liquids (see Fig. 11).

Approaching T_g, the frequency shift of the relaxation frequency increases by one order of magnitude (see Fig. 13). This is due to the finite-size effect already discussed for the 3D-confined droplets, i.e., due to a faster molecular reorienation close to T_g. However, only at the highest porosity the measured effective relaxation frequencies can be attributed to the confined liquid. At lower porosities and diameters two effects are superposed: (i) a dominant frequency shift due to a faster molecular reorienation and (ii) a frequency shift due to dielectric heterogeneity of the matrix-filler system (2D-3D), that cannot be corrected by an effective medium analysis. Nevertheless, the glass transition temperature has been approximately determined by fitting Eq. (27) to the experimental data [100 s $= \tau(T_g)$]. The shift $\Delta T_g = T_g^{\mathrm{bulk}} - T_g^{\mathrm{confined}}$ is displayed in Fig. 7. In the case of 3D-confined droplets the effective medium analysis resulted in T_g values which were about 4–5 K lower than the effective ones. So we can expect that the corrections for the 2D-3D confinement do not exceed 4 K. As indicated by the arrows and the dashed line, the corrections would change the slope $\partial\Delta T_g/\partial d$ but would only weakly affect the intersection with the x axis. Therefore, the pore diameter for which the finite-size effect disappears has been determined correctly. For a further discussion we refer to the summary.

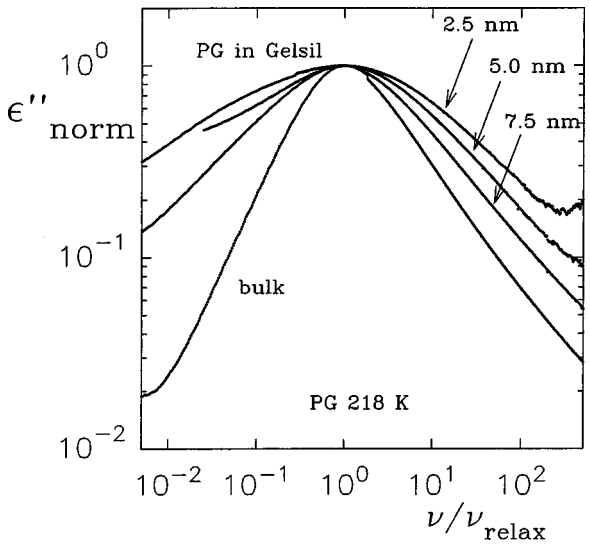

FIG. 14. Imaginary part of the normalized permittivity $\varepsilon''/\varepsilon''_{\mathrm{max}}$ vs normalized frequency ($\nu_{\mathrm{relax}} = \nu_p$ or $\nu_{\mathrm{relax}} = \nu_{\mathrm{eff}}$, respectively) for the α relaxation of bulk propylene glycol as well as for PG in porous Gelsil glasses (see Fig. 13).

Now let us have a look at the form of the relaxation process far above T_g, where no finite-size effects are expected (see Fig. 14). First we discuss the relaxation for $d = 7.5$ nm, i.e., for the highest porosity, where the above analysis suggests a 2D topology. However, compared to the bulk liquid the slopes on the high and the low frequency side change resulting in a broadening. It is as strong as for the 3D-confined droplets, although one dimension less is confined (see Fig. 8). Therefore, it is unlikely that a finite-size effect or dielectric heterogeneity of the effective medium contribute markedly. As in the case of the droplets, we attribute the broadening to a distribution of relaxation times due to nonuniform interaction with a layer of directly surface attached molecules.[6,8–10,18] Obviously, the interaction is less homogeneous or much stronger than in the hydrophobic rubber. With decreasing porosity and pore size the surface to volume ratio increases so that the broadening should increase, which is in fact observed (Fig. 14). Note that at low porosities also dielectric heterogeneity of the 2D-3D topology can yield a small contribution (see Fig. 4 for asymmetric relaxations in 3D confinements). The half width of the peak increases continuously with decreasing temperature, and at least close to T_g an additional finite-size effect cannot be excluded.[10,11] However, the change of shape is mainly caused by a surface effect and a lubrication of the inner surfaces, as it is described in Ref. 6, should result in a decrease of the broadening.

Summarizing, porous Gelsil glasses do not represent a well-defined confining medium, since (i) their topology changes from a 2D to an intermediate 2D-3D state with de-

creasing porosity or pore size and (ii) the interaction with the (uncoated) surface is much stronger than in the case of the hydrophobic rubber used as a 3D confinement. The use of simpler microstructures such as straight pores parallel to the field would guarantee a true 2D confinement that is much easier to analyze [Eq. (3) is exact for $A \to 0$]. Despite the above difficulties it was possible to provide direct evidence for a finite-size effect yielding a faster molecular relaxation at temperatures below $T_g + 50$ K. No density effects were observed and the interaction with surface attached molecules mainly affects the shape of the α relaxation.

III. 1D CONFINEMENT

In free standing films, films on substrates, or multilayer structures the material is only confined in one dimension [see Fig. 1(d)]. When the layers are orientated perpendicular or parallel to the applied field, Eq. (3) applies. In the corresponding limits $A=1$ and $A=0$, it simplifies to a simple series or parallel circuit, respectively, and it is exact for all filling factors $0 \leqslant f \leqslant 1$. The same holds for Eqs. (7) and (8) which apply for symmetric relaxations.

For the parallel orientation, $A=0$, the characteristics resemble those of a 2D confinement: the effective system directly reflects the properties of the inclusions $\varepsilon_{\text{eff}} = (1-f)\varepsilon_m + f\varepsilon_p$. Shape and position of the loss peak remain unchanged, and the measured effective relaxation strength is proportional to $\Delta\varepsilon_p$: $\Delta\varepsilon_{\text{eff}} = f\Delta\varepsilon_p$. The perpendicular orientation, $A=1$, yields effective properties that are similar to those of a 3D confinement (see Sec. I): a maximum frequency shift is obtained [Eqs. (7) and (26)], the shape of asymmetric relaxations is altered, and for large $\Delta\varepsilon_p$ the effective relaxation strength becomes independent of the intrinsic one.

IV. SUMMARY

The effective properties of confined materials are sensitive with respect to the microstructure and differ considerably depending on the number of confined dimensions. In 3D confinements dielectric heterogeneity of the effective medium gives rise to an increase of the effective relaxation frequency compared with the bulk relaxation and to a strong decrease of the relaxation strength. The effects weaken with increasing disorder or filling factor. In the limit of strongly polar fillers, $\Delta\varepsilon_{\text{eff}}$ becomes independent of the intrinsic relaxation process and depends only on the spatial distribution of the particles. The shape of the relaxation peak is approximately preserved in the case of symmetric relaxations, while for asymmetric relaxations a strong broadening is observed (in the time domain this corresponds to an altered nonexponential decay of polarization). In 2D-confined systems the parallel components dominate the dielectric response, so $\Delta\varepsilon_{\text{eff}} \propto \Delta\varepsilon_p$ holds and some characteristics of the intrinsic filler relaxation are preserved: the relaxation frequency and the shape of the relaxation peak on its low frequency side. Depending on their orientation parallel or perpendicular to the applied field, 1D-confined films behave similar to 2D- or 3D-confined materials.

Experimental data on 2D- and 3D-confined PG's has been analyzed and effects of dielectric heterogeneity were separated from finite-size and surface effects. A markedly reduced density could be excluded. While the 3D confinement consisting of randomly distributed droplets in butyl rubber exhibits a well-defined microstructure at all droplet sizes, porous Gelsil glasses show a transition from a 2D to a 2D-3D topology with decreasing porosity and pore size. In both systems nonuniform interaction with the surface or directly surface attached molecules causes a distribution of relaxation times and thus a broadening of the α relaxation, but it does not affect the main relaxation frequency of the inner molecules. For $T \leqslant T_g + 50$ K the α relaxation becomes faster than that of the bulk liquid, so that the glass transition temperature is lowered. Figure 7 clearly shows that size effects in 3D confinements are stronger than in systems where only two dimensions are confined. Although the uncertainty of the effective medium correction for the intermediate 2D-3D topology at low porosities affects the slope $\partial \Delta T_g / \partial d$, the diameter above which this finite-size effect vanishes is determined correctly. As the comparison of 2D and 3D confinement shows, it does not depend on geometrical details or chemical nature of the matrix but is a characteristic length scale for the dynamics in PG.

ACKNOWLEDGMENTS

The author is grateful to G. Nimtz, P. Pissis, and A. Spanoudaki for stimulating discussions. This work was financially supported by the ''Deutsche Forschungsgemeinschaft'' (DFG Project No. Ni 149/22-2).

[1] J. M. Drake and J. Klafter, Phys. Today **43** (5), 46 (1990).
[2] K. L. Ngai and A. K. Rizos, in *Structure and Dynamics of Glasses and Glass Formers*, edited by C. A. Angel *et al.*, MRS Symposia Proceedings No. 455 (Materials Research Society, Pittsburgh, 1997), pp. 147–150.
[3] P. Pissis, D. Daoukaki-Diamanti, L. Apekis, and C. Christodoulidis, J. Phys.: Condens. Matter **6**, L325 (1994).
[4] C. L. Jackson and G. B. McKenna, J. Non-Cryst. Solids **131-133**, 221 (1991).
[5] J. Schüller, R. Richert, and E. W. Fischer, Phys. Rev. B **52**, 15 232 (1995).
[6] M. Arndt, R. Stannarius, H. Groothues, E. Hempel, and F. Kremer, Phys. Rev. Lett. **79**, 2077 (1997).
[7] R. Böhmer, Curr. Opin. Solid State Mater. Sci. **3**, 378 (1998).
[8] G. Barut, P. Pissis, R. Pelster, and G. Nimtz, Phys. Rev. Lett. **80**, 3543 (1998).
[9] P. Pissis, A. Kyritsis, G. Barut, R. Pelster, and G. Nimtz, J. Non-Cryst. Solids **235-237**, 444 (1998).
[10] P. Pissis, A. Kyritsis, D. Daoukaki, G. Barut, R. Pelster, and G. Nimtz, J. Phys.: Condens. Matter **10**, 6205 (1998).
[11] D. Daoukaki, G. Barut, R. Pelster, G. Nimtz, P. Pissis, A. Kyritsis, and P. Pissis, Phys. Rev. B **58**, 5336 (1998).
[12] J. Dobbertin, A. Hensel, and C. Schick, J. Therm. Anal. **47**, 1027 (1996).
[13] X. Yan, C. Streck, and R. Richert, in *Dynamics in Small Confining Systems III*, edited by J. M. Drake, J. Klafter, and R. Kopel-

man, MRS Symposia Proceedings No. 464 (Materials Research Society, Pittsburgh, 1997), pp. 33–44.
[14] J. A. Forrest, K. Dalnoki-Veress, J.R. Stevens, and J. R. Dutcher, Phys. Rev. Lett. **77**, 2002 (1996).
[15] E. V. Russell, N. E. Israeloff, L. E. Walther, and H. A. Gomariz, Phys. Rev. Lett. **81**, 1461 (1998).
[16] A. Arbe, J. Colmenero, M. Monkenbusch, and D. Richter, Phys. Rev. Lett. **81**, 590 (1998).
[17] F. M. Aliev and G. P. Sinha, Mol. Cryst. Liq. Cryst. **303**, 325 (1997).
[18] C. Streck, Yu. B. Mel'nichenko, and R. Richert, Phys. Rev. B **53**, 5341 (1996).
[19] P. Marquardt, G. Nimtz, and W. Weiss, J. Phys. A **20**, L619 (1987).
[20] G. Adams and J. H. Gibbs, J. Chem. Phys. **43**, 139 (1965).
[21] J. Monecke, Phys. Status Solidi B **154**, 805 (1989).
[22] G. Bánhegyi, Colloid Polym. Sci. **264**, 1030 (1986).
[23] R. Pelster and U. Simons, Colloid Polym. Sci. **277**, 2 (1999).
[24] R. H. Cole and K. S. Cole, J. Chem. Phys. **9**, 341 (1941).
[25] C. J. F. Böttcher, *Theory of Electric Polarisation* (Elsevier, Amsterdam, 1952).
[26] H. Fröhlich, *Theory of Dielectrics* (Clarendon, London, 1949).
[27] A. K. Jonscher, *Dielectric Relaxation in Solids* (Chelsea Dielectrics, London, 1983); *Universal Relaxation Law* (Chelsea Dielectrics, London, 1996).
[28] G. Bánhegyi, Colloid Polym. Sci. **266**, 11 (1988); **264**, 1030 (1986).
[29] L. K. H. van Beek, in *Progress in Dielectrics*, edited by J. B. Birks (Heywood, London, 1967), Vol. 7, pp. 69–114.
[30] S. S. Dukhin, in *Surface Colloid Science*, edited by E. Matijevic (Interscience, New York, 1971), Vol. 3, pp. 83–165.
[31] The increase of the relaxation frequency in heterogeneous mixtures with a polar constituent has already been noticed in early studies, although it has not been quantified [G. P. De Loor, Appl. Sci. Res., Sect. B **11**, 310 (1965)]. For $\alpha=0$ Eq. (7) was also obtained by Jäckle [Eq. (7) in Ref. 13].
[32] D. R. McKenzie and R. C. McPhedran, Nature (London) **265**, 128 (1977); Proc. R. Soc. London, Ser. A **359**, 45 (1978).
[33] W. T. Doyle, J. Appl. Phys. **49**, 795 (1978).
[34] L. Fu and L. Resca, Phys. Rev. B **47**, 16 194 (1993).
[35] L. Fu, P. B. Macedo, and L. Resca, Phys. Rev. B **47**, 13 818 (1993).
[36] S. Sheu, S. Kumar, and R. I. Cukier, Phys. Rev. B **42**, 1431 (1990).
[37] S. Havriliak and S. Negami, J. Polym. Sci., Part C: Polym. Symp. **14**, 99 (1966).
[38] F. Stickel, E. W. Fischer, and R. Richert, J. Chem. Phys. **104**, 2043 (1996).
[39] G. Barut, Ph.D. thesis, University of Cologne, Germany, 1996.
[40] R. Pelster, A. Kops, G. Nimtz, A. Enders, H. Kietzmann, P. Pissis, A. Kyritsis, and D. Woermann, Ber. Bunsenges. Phys. Chem. **97**, 666 (1993).
[41] H. G. Krauthäuser and G. Nimtz, J. Mol. Struct. **383**, 315 (1996).
[42] R. Pelster, IEEE Trans. Microwave Theory Tech. **43**, 1494 (1995).
[43] F. Alvarez, A. Algegría, and J. Colmenero, Phys. Rev. B **47**, 125 (1993).
[44] R. Hilfer, Phys. Rev. B **44**, 60 (1991).
[45] R. Hilfer, B. Nøst, E. Haslund, Th. Kautsch, B. Virgin, and B. D. Hansen, Physica A **207**, 19 (1994).
[46] W. Niesel, Ann. Phys. (Leipzig) **10**, 336 (1952).
[47] S. Stölzle, A. Enders, and G. Nimtz, J. Phys. I **2**, 401 (1992).
[48] S. Stölzle, A. Enders, and G. Nimtz, J. Phys. I **2**, 1765 (1992).
[49] M. J. Benham, J. C. Cook, J-C. Li, D. K. Ross, P. L. Hall, and B. Sarkissian, Phys. Rev. B **39**, 633 (1989).
[50] P. W. Schmidt, A. Höhr, H.-B. Neumann, H. Kaiser, D. Avnir, and J. S. Lin, J. Chem. Phys. **90**, 5016 (1989).
[51] P. K. Dixon, Phys. Rev. B **42**, 8179 (1990).